Exploring the binding properties and structural stability of an opsin in the chytrid *Spizellomyces punctatus* using comparative and molecular modeling

Steven R. Ahrendt[1,2,3†], Edgar M. Medina[4,5], Chia-en A. Chang[2,6], and Jason E. Stajich[1,2 *]

[1]Department of Plant Pathology & Microbiology
University of California-Riverside
Riverside, California 92521

[2]Institute for Integrative Genome Biology
University of California-Riverside
Riverside, California 92521

[3]Graduate program in Genetics, Genomics, and Bioinformatics
University of California-Riverside
Riverside, California 92521

[4]Department of Biology
Duke University
Durham, North Carolina 27708

[5]Center for Genomic and Computational Biology
Duke University
Durham, North Carolina, 27710

[6]Department of Chemistry,
University of California-Riverside
Riverside, California 92521

[†] Present address:
DOE Joint Genome Institute,
Walnut Creek, CA 94598

[*]Corresponding Author: Jason E. Stajich jason.stajich@ucr.edu

PeerJ Preprints | https://doi.org/10.7287/peerj.preprints.2397v2 | CC BY 4.0 Open Access | rec: 25 Jan 2017, publ: 25 Jan 2017

Abstract

Background. Opsin proteins are seven transmembrane receptor proteins which detect light. Opsins can be classified into two types and share little sequence identity: type 1, typically found in bacteria, and type 2, primarily characterized in metazoa. The type 2 opsins (Rhodopsins) are a subfamily of G-protein coupled receptors (GPCRs), a large and diverse class of seven transmembrane proteins and are generally restricted to metazoan lineages. Fungi use light receptors including opsins to sense the environment and transduce signals for developmental or metabolic changes. Opsins characterized in the Dikarya (Ascomycetes and Basidiomycetes) are of the type 1 bacteriorhodopsin family but the early diverging fungal lineages have not been as well surveyed. We identified by sequence similarity a rhodopsin-like GPCR in genomes of early diverging chytrids and examined the structural characteristics of this protein to assess its likelihood to be homologous to animal rhodopsins and bind similar chromophores.

Methods. We used template-based structure modeling, automated ligand docking, and molecular dynamics to assess the structural and binding properties of an identified opsin-like protein found in *Spizellomyces punctatus*, a unicellular, flagellated species belonging to Chytridiomycota, one of the earliest diverging fungal lineages. We tested if sequence and inferred structure were consistent with a solved crystal structure of a type 2 rhodopsin from the squid *Todarodes pacificus*.

Results. Our results indicate that the *Spizellomyces* opsin has structural characteristics consistent with functional animal type 2 rhodopsins and is capable of maintaining a stable structure when associated with the retinaldehyde chromophore, specifically the 9-*cis*-retinal isomer. Together, these results support further the homology of *Spizellomyces* opsins to animal type 2 rhodopsins.

Discussion. This represents the first test of structure/function relationship of a type 2 rhodopsin identified in early branching fungal lineages, and provides a foundation for future work exploring pathways and components of photoreception in early fungi.

Keywords: Chytrid; Opsin; Homology Modeling; Light receptor; Protein structure; GPCR Early diverging fungi; Evolution; Mycology

Introduction

An organism experiences a multitude of environmental stimuli including chemical, gravity, the Earth's magnetic field, pressure, and light. The biochemical ability to appropriately process and respond to these signals is a complex and involved task, and understanding the molecular mechanisms of these responses is an ongoing scientific challenge. The presence or absence of light is perhaps one of the easiest sources of stimuli to comprehend and observe. The daily cycles of sunlight due to the rotation of the planet has had a profound influence on the

PeerJ Preprints | https://doi.org/10.7287/peerj.preprints.2397v2 | CC BY 4.0 Open Access | rec: 25 Jan 2017, publ: 25 Jan 2017

development of life that it comes as no surprise to find some form of photoreception in nearly every organism on the planet. The widespread occurrence of such an ability, however varied in its implementation, speaks to its importance during the earliest stages of development of life.

In Fungi, there are several classes of proteins capable of photoreception that function by different mechanisms of action and have varied structures, sensitivities, and specializations. These include blue light responsive white-collar complex, VIVID and cryptochrome photoreceptors, red light responsive phytochromes, and multi-wavelength light responsive opsins (Idnurm, Verma, & Corrochano, 2010). The opsins are a large class of seven-transmembrane proteins which bind retinylidene compounds required for photoreception and can be subdivided into Types 1 or 2 based on phylogenetic history, sequence similarity, and function. The classes share some characteristics in structure (i.e. seven helical transmembrane domains) and mechanism of activation (i.e. photoisomerization of a retinaldehyde chromophore) but have distinct evolutionary histories (Spudich et al., 2000).

Opsins are part of the large G-protein coupled receptor (GPCR) superfamily, which has more than 800 distinct described members in humans (Lagerström & Schiöth, 2008). GPCR proteins share a similar architecture: seven membrane-spanning helical regions connected by three intracellular and three extracellular loop regions. The cytoplasmic region of the GPCR interacts with heterotrimeric G proteins found on the intracellular side of the plasma membrane, which in turn function in signal transduction (Neves, Ram, & Ivengar, 2002). Of the five major GPCR families, the Class-A family, comprising the opsins, various neurotransmitters, and hormone receptors, is by far the largest with approximately 700 proteins classified into four subfamilies (Katritch, Cherezov, & Stevens, 2013).

The "Type 2 rhodopsins" represent a small subgroup of the opsin subfamily of Class-A GPCRs. Unlike other members of this class, they are activated by the interaction between a single photon of light and a covalently bound chromophore. A functional rhodopsin (rhodopsin pigment) is generated when an opsin apoprotein forms a covalent bond with a retinaldehyde chromophore via a Schiff-base linkage at a conserved lysine residue. While 11-*cis*-retinal is the most common chromophore observed in vertebrates and invertebrates, additional types are also found in nature. For example, 3,4-dehydroretinal is observed in fish, amphibians, and reptiles. Switching between the 11-*cis*- and 3,4-dehydro- chromophores can be employed as a light adaptation strategy in certain freshwater fish (Shichida & Matsuyama 2009). 3-hydroxyretinal is found in insects, while 4-hydroxyretinal is observed in the firefly squid. In addition to the 11-*cis*-conformation, retinal can adopt a number of different isomers, including all-*trans*-, 13-*cis*-, and 9-*cis*- (Shichida & Matsuyama 2009). Previous studies using hybrid quantum mechanics/molecular mechanics (QM/MM) simulations suggest that the 11-*cis*-retinal isomer has been evolutionarily selected as the optimal chromophore due to the energetic stability of the resulting chromophore-opsin pigment (Sekharan & Morokuma, 2011).

Activation of the rhodopsin occurs through the photoisomerization of 11-*cis*-retinal to all-*trans*-retinal, which causes a conformational change in the protein structure of the receptor. Alternatively, the ion transporter rhodopsins (part of the "Type 1 opsins") are activated by the

PeerJ Preprints | https://doi.org/10.7287/peerj.preprints.2397v2 | CC BY 4.0 Open Access | rec: 25 Jan 2017, publ: 25 Jan 2017

photoisomerization of all-*trans*-retinal to 13-*cis*-retinal. These function as membrane channels and are typically used for light-driven membrane depolarization via proton or chloride ion pumping. Examples of this group can be found in bacteria, archaea, and eukaryotes, and include the bacterial sensory rhodopsins, channelrhodopsins, bacteriorhodopsins, halorhodopsins, and proteorhodopsins (Zhang et al., 2011). The nature of the evolutionary relationship between the two types of rhodopsin has not been definitively established and is currently the subject of discussion (Terakita, 2005; Shichida & Matsuyama 2009; Becker et al., 2016; Devine, Theobald, & Oprian, 2016).

There are at least three distinct phyla of early diverging fungi which are often referred to as "zoosporic fungi" or, more informally, "chytrids": the Cryptomycota, Chytridiomycota, and Blastocladiomycota (James et al., 2006; Stajich et al., 2009; Jones et al., 2011; James et al., 2013). These lineages share as a defining characteristic the presence of a flagellated life stage called a zoospore. Previous work has demonstrated that some species in these early diverging lineages are phototaxic. For example, the marine chytridiomycete *Rhizophydium littoreum* will respond to light at a variety of wavelengths, with the most rapid response occurring at 400 nm (Muehlstein, Amon, & Leffler, 1987). While the evidence strongly suggests blue-light sensitivity, the researchers did not specifically characterize the active photoreceptor. Similarly, zoospores from the blastocladiomycete *Allomyces reticulatus* were determined not only to be phototactic, but also to possess visible, red-pigmented eyespots in which the photosensitive proteins are localized (Saranak & Foster, 1997). Careful analysis determined that the action spectrum of the phototactic *A. reticulatus* zoospores peaks at 536 +/- 4 nm, similar to that of the human green-sensitive cone. More recently, comprehensive work on the related blastocladiomycete *Blastocladiella emersonii* demonstrated that a type 1 rhodopsin is in part responsible for phototaxis in response to green light (522 nm) (Avelar et al. 2014).

An initial analysis of the chytrid *Batrachochytrium dendrobatidis* genome revealed a surprising finding of a GPCR protein with similarity to the rhodopsin superfamily. Searches of additional genomes of early diverging fungi, including the saprotrophic chytrid *Spizellomyces punctatus,* revealed the presence of rhodopsin-like proteins in multiple zoosporic fungal lineages. The availability of these examples of opsin homologs in the deeply diverging fungal lineages suggested the shared ancestry of these light sensing receptors and the presence of this pathway in the fungal-animal ancestor (Krishnan et al., 2012; Medina EM, unpublished data).

The growing availability of x-ray structures of different GPCRs has illustrated a strong similarity in overall topology (Katritch, Cherezov, & Stevens, 2013). As a result, structural models built for various GPCRs have been successful in *in silico* screening of inhibitors or examining protein dynamics (Bermudez & Wolber, 2015; Taddese et al., 2013; Ai & Chang, 2012). Comparative modeling, also known as "homology modeling", is a computational method for building a structure for a protein of interest for which the structure is unknown. It is a template-based method which acts on the target's sequence similarity to proteins for which the structure has been experimentally verified (template) (Sali, 1995). It is distinct from *ab initio* or *de novo* modeling, which instead uses only the target sequence and free-energy minimization

PeerJ Preprints | https://doi.org/10.7287/peerj.preprints.2397v2 | CC BY 4.0 Open Access | rec: 25 Jan 2017, publ: 25 Jan 2017

techniques (Bradley, Misura, & Baker, 2005). Homology modeling works best when there is high sequence identity between the target and template. Protein targets with sequence identity levels <30% with their template structure are often referred to as being in the "Twilight zone" of homology modeling, where models generated from these alignments are not of the highest quality (Chung & Subbiah, 1996). Coupled with molecular dynamics (another computational technique used to simulate interactions of complex molecules at the atomic level) and molecular docking (used to simulate protein-ligand interactions), homology modeling has multiple applications including structure-based drug discovery and investigations of protein dynamics.

The opsin-like proteins identified in the genomes of early diverging chytrid fungi are sufficiently similar to experimentally verified animal opsin structures for modeling and hypothesis testing about the potential ligand binding. We selected the *Spizellomyces punctatus* opsin-like GPCR for investigation as it possessed a conserved lysine residue suitable for retinal binding, unlike those in other chytrids. The target sequences and the rhodopsin homologs were modeled with Type 2 rhodopsin crystal structure templates made possible by the growing number of GPCR structures from the rhodopsin subfamily in the PDB (Katritch, Cherezov, & Stevens, 2013). We generated a homology model for an opsin-like GPCR identified in the *S. punctatus* and use it to explore the binding properties of retinal isomers, the functional chromophores in rhodopsin-mediated photosensing. Here we show that the *S. punctatus* opsin is structurally similar to functional animal type 2 rhodopsins and is stable when associated with a 9-*cis*-retinal chromophore.

Materials & Methods

Sequence identification and homology modeling

Putative rhodopsin sequences in early diverging fungal lineages were identified based on sequence similarity to the Profile Hidden Markov model from the Pfam database (Finn et al., 2014), accession PF00001 ("7tm_1"). The HMM was searched against the predicted proteins from *S. punctatus*, *B. dendrobatidis*, *A. macrogynus* HMMER v3.0 (Eddy, 2011) using e-value cutoff 1e-10. Inspection of the protein sequence of the *S. punctatus* homolog revealed a putative truncation, which lead us to correct the gene model at locus SPPG_00350 by adding a missing cytosine in the genome at position 1041 of the locus. The discrepancy was identified using exonerate (Slater & Birney, 2005) alignment of chytrid proteins to the genome to identify and correct this single deletion in the genome assembly (Supplemental file; https://github.com/stajichlab/chytropsin). The amended protein sequence SPPG_00350T0L was used for subsequent analyses. The *S. punctatus* protein structure model was constructed using the I-TASSER server with the provided GPCR specific library (Zhang, 2010). The normalized z-scores, indicative of alignment quality, of the top ten threading templates used by I-TASSER are provided in Table S2. Additionally, manual correction of the K320 orientation was performed by energy minimization using the general Amber force field (GAFF) (Wang et al., 2004) in Avogadro (Hanwell et al., 2012) after automatic refinement with OpusROTA. The optimal

PeerJ Preprints | https://doi.org/10.7287/peerj.preprints.2397v2 | CC BY 4.0 Open Access | rec: 25 Jan 2017, publ: 25 Jan 2017

model was selected using the I-TASSER provided "c-score", a confidence value based on the significance of threading template alignments. The rhodopsin crystal structure from *Todarodes pacificus* (PDBid 2Z73; Murakami & Kouyama, 2008) was additionally selected for subsequent docking and molecular dynamics experiments. Stereochemical properties of both protein structures were validated using PROCHECK (v3.5) (Laskowski et al., 1993; Wiederstein & Sippl, 2007), ProQM (Ray, Lindahl, & Wallner, 2010), and Verify3D (Lüthy, Bowie, & Eisenberg, 1992). The *S. punctatus* homology model structure file is available on Github at http://github.com/stajichlab/chytropsin/.

Docking and Molecular dynamics (MD)

Automated protein-ligand docking was accomplished using Autodock 4 (Morris et al., 2009) and implementing a Lamarckian genetic algorithm approach for calculating the minimum free energy of binding of small molecules. Small molecule files were obtained from PubChem (Bolton et al., 2008) for the following isomers of retinal: 11-*cis* (A1), all-*trans*, 9-*cis*, 13-*cis*, 3,4-dehydro (A2), 3-hydroxy (A3), and 4-hydroxy (A4) used in the covalent docking screen. A covalent linkage was formed by manually specifying the presence of a bond between the terminal carbon atom in retinal and terminal nitrogen atom in the lysine side chain. The specific lysine predicted to be involved in Schiff-base linkage with the chromophore was inferred through multiple sequence alignment.

The dynamics of both the *Todarodes* and *Spizellomyces* rhodopsin complexes were investigated using all-atom molecular dynamics simulations with the Amber14 suite of programs (Case et al., 2015). Due to the computational expense of an explicit solvation model for simulating water molecules, an implicit solvation model (Onufriev, Bashford, & Case, 2000) (modified from the generalized Born solvation model (Bashford & Case, 2000)) was used in AMBER with the *igb=2* flag. The all atom force-field ff14SB (Hornak et al., 2006) was used as implemented in AMBER14, and GAFF was implemented for the ligand. Additionally, in order to mimic a membrane in which the protein would be found *in vivo,* all residues belonging to the transmembrane helices, except those within the binding pocket, were restricted using the *restraint* flag. Initial minimization was performed for 1ns, followed by three NVT equilibration steps for 50ps progressing from 200K to 250K to 298K. The final production simulation was run for 100ns at 298K. For comparison, the photoisomerization of 11-cis-retinal to all-trans configuration occurs on the order of 200 fs (Smith 2010).

For simulations of the squid structure, PDBid 2Z73 was used along with the structure of 11-*cis*-retinal crystallized with it. For the *S. punctatus* structure, simulations were performed using 9-*cis*-retinal ligand in the lowest energy conformation. 9-*cis*-retinal was chosen based on the covalent docking screen results. Backbone atoms were kept rigid while binding pocket residues were made flexible. Trajectory visualization and RMSD analysis were accomplished using VMD (v1.9.1) (Humphrey, Dalke, & Schulten, 1996). Potential energy of the system was summarized using the *process_mdout.perl* script, provided with the AMBER package.

PeerJ Preprints | https://doi.org/10.7287/peerj.preprints.2397v2 | CC BY 4.0 Open Access | rec: 25 Jan 2017, publ: 25 Jan 2017

Results

Structural quality of homology model

For this study, a template-based model was constructed for the *S. punctatus* protein sequence using the I-TASSER website and GPCR specific database. Top BlastP hits of the *S. punctatus* protein to the PDB (as of 2016) include numerous opsin proteins, with the top scoring hit at 22.5% identity to a rhodopsin from *Bos taurus* (Table S1). Templates predicted by I-TASSER included both chains of the *T. pacificus* rhodopsin protein (Table S2). The *S. punctatus* protein shares 22% sequence identity with the *T. pacificus* sequence and several key functional and structural motifs are conserved between the structures (Figure 1).

The binding pocket comprises a number of hydrophobic residues which provide a sterically restrictive space in which the retinal ligand is situated (orange). The major functional residues in this group are the conserved lysine (cyan) and counterion (red) which facilitate proton transfer during photoisomerization. The ionic lock motif contains an (E/D)RY and NPxxY motif, which together act as a structural support which stabilizes the protein in the inactive ("dark") state, and is broken upon receptor activation (Smith 2010). In *S. punctatus*, the (E/D)RY and NPxxY motifs are both functionally conserved as 115ERY117 and 326NPVLF330 (pink). Two additional linkages are responsible for correct protein folding: a conserved disulfide bond between C110-C187, and a conserved salt bridge between R117-D190. *S. punctatus* model possesses both of these motifs as C91-C166 (yellow), and potentially R158-D169 (purple).

The quality of the *S. punctatus* homology model was assessed with Ramachandran plots (Ramachandran, Ramakrishnan, & Sasisekharan, 1963), generated using PROCHECK (Laskowski et al., 1993; Wiederstein & Sippl, 2007), which graphically display the backbone dihedral angles (φ and ψ) of each amino acid residue in a protein. An aggregate assessment of observed protein structures determined by x-ray crystallography defines regions of acceptable stereochemistry; here using observed phi-psi distribution for 121,870 residues from 463 known X-ray protein structures. In practice, this analysis can be used for structure validation. A model with more than 90% of its residues having favorable stereochemistry is considered to be of good quality. For *S. punctatus*, the percentage of residues which fell within the most favorable region was 85.4%. The *T. pacificus* crystal structure of rhodopsin (Murakami 2008) has a score of 90.9% in this category (Figure S1).

Additionally, Verify3D (Lüthy, Bowie, & Eisenberg, 1992) was used to assess model quality. Structures modeled correctly will have higher scores than structures which have been modeled incorrectly. Here, the *S. punctatus* model generated using the I-TASSER+GPCR database had a final score of 72.41, and 46.32% of the residues had an averaged 3D-1D score >= 0.2. For comparison, the rhodopsin x-ray crystal structure from *T. pacificus* had a final score of 87.85, and 58.86% of residues had a profile score >= 0.2. To provide further support that the *S. punctatus* model was constructed correctly, a model was generated with the *S. punctatus* sequence using the sensory rhodopsin II x-ray crystal structure from the archaeon *Natronomonas pharaonis* (PDBid 1H68, Royant et al., 2001), a type 1 opsin and thus a presumed incorrect

PeerJ Preprints | https://doi.org/10.7287/peerj.preprints.2397v2 | CC BY 4.0 Open Access | rec: 25 Jan 2017, publ: 25 Jan 2017

modeling target. In this reconstruction, the final score was 15.08, and only 19.57% of residues had a Verify3D score >= 0.2. When the scores for these proteins are plotted as a function of their sequences (Figure S2) the average scores fall between -0.12 and 0.66 (Figure S2B) and -0.19 and 0.87 (Figure S2A). The average scores for the *S. punctatus* structure model constructed against 1H68 however fall between -0.56 and 0.49 (Figure S2C).

Finally, ProQM (Ray, Lindahl, & Wallner, 2010) was used to assess model quality, providing a score between 0 (poor) and 1 (correctly modeled). The *S. punctatus* model had a global quality score of 0.5 and a range of local quality scores 0.03 to 0.91, with low scores corresponding to loop regions (Figure S2A). The *T. pacificus* crystal structure had in general higher local quality scores, with a range of 0.11 to 1.13 and a global quality score of 0.766 (Figure S2B). The quality assessment of the presumed mis-modeled *S. punctatus* homology model (described above) again suggested it was poorly modeled, with a global quality score of 0.42 and a range of local quality scores from -0.18 to 0.96 (Figure S4C).

Computational ligand screen

Rhodopsin functions through the use of a retinaldehyde chromophore. The most common chromophore observed in both invertebrates and vertebrates is 11-*cis*-retinal (Shichida & Matsuyama, 2009). This retinal isomer is also used in the *T. pacificus* rhodopsin association. To determine if the *S. punctatus* rhodopsin utilized the same isomeric configuration of retinal, computational protein-ligand docking was performed using Autodock 4 with 11-*cis*-retinal and other vitamin-A based retinaldehyde compounds. The compounds 11-*cis*-retinal, all-*trans*-retinal, 9-*cis*-retinal, 13-*cis*-retinal, 3,4-dihydroretinal, 3-hydroxyretinal, and 4-hydroxyretinal were tested (Figure 2) and all have demonstrated activity in nature. When docked against the squid crystal structure, 11-*cis*-retinal had the lowest free energy of binding, as expected since this is the functional chromophore for the squid rhodopsin protein. Ranking the energy scores, all-*trans*-retinal had the highest free energy of binding. For the *S. punctatus* modeled structure, the lowest energy conformations were observed when bound to 9-*cis*-retinal isomer, with the next lowest conformations observed with the 11-*cis*-retinal isomer. The results of the initial pre-Molecular Dynamics (MD) docking screen are provided in Table 1.

To assess the flexibility of the predicted *S. punctatus* + 9-*cis*-retinal complex, molecular dynamics simulations on the opsin and unbound chromophore using AMBER 14 were performed and compared to that of the canonical squid + 11-*cis*-retinal complex. An overview of the potential energy of two systems during the 100ns simulation is given in Figure 3A. While the potential energy of the *S. punctatus* complex is much lower than that of the squid, both complexes are extremely stable over the long term. Using VMD to plot the RMSD relative to the averaged structure for both complexes also suggests they are stable. For both complexes, these results are given in Figure 3B. The RMSD of the squid complex begins around 1.5Å and ends close to 0.7Å during the simulation, with a mean and standard deviation of 0.87±0.21Å. The *S. punctatus* complex fluctuates between 2.56Å and 8.92Å, with a mean and standard

PeerJ Preprints | https://doi.org/10.7287/peerj.preprints.2397v2 | CC BY 4.0 Open Access | rec: 25 Jan 2017, publ: 25 Jan 2017

deviation of 4.67±1.07Å. Additionally, the per-residue RMSD for both structures remains low during the course of the simulation (Figure S3).

The binding pockets of both receptor proteins were characterized using the fpocket webservice (http://fpocket.sourceforge.net) (Le Guilloux, Schmidtke, & Tuffery, 2009). This analysis suite generates clusters of spheres to describe pockets identified in a given protein. The pockets predicted within the center of the protein are displayed in Figure 4 A-D, before and after the MD simulations. The pocket for the *T. pacificus* rhodopsin, remains quite compact prior to (Figure 4A) and after simulation (Figure 4B). The *S. punctatus* pocket is consistently larger than that of *T. pacificus* during the course of the simulation (Figure 4C-D). In the unbound state, the average of the distances from the center of mass of the retinal ligand to each of the Cα of binding pocket residues in the *T. pacificus* or *S. punctatus* structures did not change substantially during the course of the simulation, though there is a slight increase and noticeably more variability in the *S. punctatus* pocket. (Figure 4E).

During the course of the *S. punctatus* simulation, the 9-*cis*-retinal ligand shifts approximately 1.6Å inside the binding pocket of the model. A shift of approximately 1.8Å by the functional nitrogen atom can be observed during the simulation. The ion lock distance (between E116 and R250) remained consistent, decreasing only slightly from 3.5Å to 3.4Å, while the disulfide bond distance (cysteine - cysteine link between C91 and C166) decreased from 5.4Å to 3.7Å (Figure 5). During the *T. pacificus* simulation, both the 11-*cis*-retinal ligand shift by less than 1Å, and the conserved unbound lysine residue (K296) maintains its linear conformation. The *T. pacificus* ion lock and disulfide distances and orientations remained relatively unchanged, potentially due to the *T. pacificus* structure being closer to optimal conformation initially.

To assess any potential improvements in docking scores, revised covalent docking was performed using the structures resulting from the previously described simulations and the ligands presented in Figure 1. Table 1 provides the initial and revised measures of free energy for each docking run, and Table S3 provides energy terms of the ligands and all energy terms for each of the lowest docked runs. For *S. punctatus* the measures of free energy using the structures from the end of the simulation (frame 3) were lowest when using 13-*cis* and 9-*cis* isomers of retinal (-1.76 and -1.83 kcal/mol, respectively), with the 11-*cis* isomer as the next lowest (-1.49 kcal/mol). For *T. pacificus* all isomers were relatively similarly low-scoring, although with slight increases using models near the end of the simulation.

Discussion

Using the genomes of early-diverging chytrid fungi *B. dendrobatidis* and *S. punctatus*, we identified putative proteins homologous to metazoan Type 2 Rhodopsins. Rhodopsin functions as a photoreceptor via a well-defined interaction between a photon of light, a retinaldehyde chromophore (observed commonly as 11-*cis*-retinal), and the GPCR opsin protein in order to initiate a cellular response through intracellularly-coupled heterotrimeric G-proteins. There is evidence to suggest that the covalent bond architecture is not biochemically necessary in experimentally manipulated Type 1 opsins (Schweiger, Tittor, & Oesterhelt, 1994). However, in

PeerJ Preprints | https://doi.org/10.7287/peerj.preprints.2397v2 | CC BY 4.0 Open Access | rec: 25 Jan 2017, publ: 25 Jan 2017

naturally occurring opsins this interaction is always facilitated by the presence of a lysine residue in the binding pocket of the GPCR to which the chromophore is covalently bound (Smith 2010). Of the putative rhodopsin proteins identified in several chytrid fungi, the candidate identified in *S. punctatus* is the most likely to function as photoreceptor. This protein is highly similar to experimentally verified metazoan rhodopsin proteins and shares structural and functional motifs including most critically the conserved lysine residue within the binding pocket.

Experimental evidence in Blastocladiomycota chytrid fungi indicates they have light regulated behavior (Avelar et al. 2014). Phototaxis has been documented in *A. reticulatus* and the responsible photoreceptor protein was deduced to be rhodopsin (Saranak & Foster, 1997). Additionally, in the entomopathogenic chytrid fungus *Coelomomyces dodgei*, photoperiod-dependent spore release has been documented, although the underlying biochemical pathway has not been clearly elucidated (Federici, 1983). The most comprehensive evidence that couples light response behavior and molecular mechanisms is in *B. emersonii*. Light perception in this fungus requires eye-spot localized photoreceptors that were determined to be fusion proteins of a type 1 rhodopsin and guanylyl cyclase (Avelar et al., 2014; Avelar et al., 2015). There is much less experimental evidence for rhodopsin-regulated behavior in Chytridiomycota. The primary observations are in *Rhizophydium littoreum*, for which there is evidence of blue-light responsive phototaxis (Muehlstein, Amon, & Leffler, 1987), but the underlying molecular mechanisms have not been explored.

In the present study we used *in silico* docking screens to assess the capacity of the *S. punctatus* opsin model to bind to known retinal ligands in order to form a functional rhodopsin complex. This sequence is currently the only Type 2 rhodopsin identified in fungi which possesses the conserved lysine and counterion residues, though more complete genomic and transcriptomic sampling of zoosporic lineages will undoubtedly identify additional instances of this gene. Based on this screen, 9-*cis*-retinal appeared to be the most favorable ligand for use by *S. punctatus*. As such, the 9-*cis* isomer was used in subsequent refinement by molecular dynamics. When compared to the squid crystal structure and its canonical 11-*cis*-retinal ligand, the *S. punctatus* + 9-*cis*-retinal complex takes longer to reach a stable conformation, and this conformation deviates quite a bit from the initial structure model. While this suggests inconsistencies with the initial homology model, both the squid and *S. punctatus* opsin+chromophore complexes appear highly stable. Different chromophores have been observed in nature in opsin complexes being utilized for different purposes. While functional binding pocket residues (e.g. lysine and counterion) are conserved, there are binding pocket residue differences between the squid and fungal structures which could account for the utilization of different chromophores. For example, fewer large hydrophobic residues in the fungal pocket might permit accommodation of different chromophores. Additionally, during the course of exploring why 11-*cis*-retinal was most often observed in mammalian systems, Sekharan and Morokuma (2011) demonstrated that, generally, 9-*cis*-retinal is only slightly less stable, and under certain conditions can in fact be more stable, than the 11-cis isomer. Our molecular docking results suggest that one preferential ordering of ligands would be: 9-*cis* > 13-

PeerJ Preprints | https://doi.org/10.7287/peerj.preprints.2397v2 | CC BY 4.0 Open Access | rec: 25 Jan 2017, publ: 25 Jan 2017

395 *cis* > 11-*cis* > 4-hydroxy > all-*trans* > 3,4-dihydro- > 3-hydroxy-retinal.While a thorough
396 treatment of the phylogenetic support for the shared ancestry of these proteins will be presented
397 elsewhere (Medina EM, unpublished data), the functional relevance of such proteins remains to
398 be explored. The *S. punctatus* + 9-*cis*-retinal complex after molecular dynamics simulations
399 supports the hypothesis that this GCPR is a functional photoreceptor and provides a foundation
400 for future work dealing with photoreception in early diverging fungi.
401
402
403 **Acknowledgements**
404 We would like to thank Zhiye Tang and Christopher Roberts for technical assistance. Genome
405 sequence and gene annotations of the *Spizellomyces punctatus*, *Allomyces macrogynus* and
406 *Batrachochytrium dendrobatidis* JEL423 strains were obtained from the Broad Institute and the
407 Origins of Multicellularity Project. Genome of the *Batrachochytrium dendrobatidis* JAM81
408 strain was obtained from the Joint Genome Institute Mycocosm database. Computations were
409 performed on the University of California-Riverside Institute for Integrative Genome Biology
410 high performance bioinformatics cluster (http://www.bioinformatics.ucr.edu/).
411

PeerJ Preprints | https://doi.org/10.7287/peerj.preprints.2397v2 | CC BY 4.0 Open Access | rec: 25 Jan 2017, publ: 25 Jan 2017

References

Ai R, Chang CE. Ligand-specific homology modeling of human cannabinoid (CB1) receptor. 2012. *Journal of Molecular Graphics and Modelling*. 38:155-164. DOI:10.1016/j.jmgm.2012.05.002.

Armougom F, Moretti S, Poirot O, Audic S, Dumas P, Schaeli B, Keduas V, Notredame C. 2006. Expresso: automatic incorporation of structural information in multiple sequence alignments using 3D-Coffee. *Nucleic Acids Research*. 34:W604–8. DOI:10.1093/nar/gkl092.

Avelar GM, Schumacher RI, Zaini PA, Leonard G, Richards TA, Gomes SL. 2014. A Rhodopsin-Guanylyl Cyclase Gene Fusion Functions in Visual Perception in a Fungus. *Current Biology*. 24:1234-1240. DOI:10.1016/j.cub.2014.04.009.

Avelar GM, Glaser T, Leonard G, Richards TA, Ulrich H, Gomes SL. 2015. A Cyclic GMP-Dependent K+ Channel in the Blastocladiomycete Fungus *Blastocladiella emersonii*. *Eukaryotic Cell.* 14:958-963. DOI:10.1128/EC.00087-15.

Bashford D, Case DA. 2000. Generalized Born models of macromolecular solvation effects. *Annual Review of Physical Chemistry.* 51:129–152. DOI:10.1146/annurev.physchem.51.1.12.

Becker EA, Yao AI, Seitzer PM, Kind T, Wang T, Eigenheer R, Shao KSY, Yarov-Yarovoy V, Facciotti MT. 2016. A Large and Phylogenetically Diverse Class of Type 1 Opsins Lacking a Canonical Retinal Binding Site. *PLoS One*. 11:e0156543. DOI:10.1371/journal.pone.0156543.

Bermudez M, Wolber G. 2015. Structure versus function – The impact of computational methods on the discovery of specific GPCR-ligands. *Bioorganic & Medicinal Chemistry.* 23:3907-3912. DOI:10.1016/j.bmc.2015.03.026.

Bradley P, Misura KMS, Baker D. 2005. Toward High-Resolution de Novo Structure Prediction for Small Proteins. *Science.* 309:1868-1871. DOI:10.1126/science.1113801.

Bolton EE, Wang Y, Thiessen PA, Bryant SH. 2008. PubChem: Integrated Platform of Small Molecules and Biological Activities. In: Wheeler RA, Spellmeyer DC, ed. *Annual Reports in Computational Chemistry*. Elsevier. 12:217–241. DOI:10.1016/S1574-1400(08)00012-1.

Case DA, Berryman JT, Betz RM, Cerutti DS, Cheatham III TE, Darden TA, Duke RE, Giese TJ, Gohlke H, Goetz AW, Homeyer N, Izadi S, Janowski P, Kaus J, Kovalenko A, Lee T, LeGrand S, Li P, Luchko T, Luo R, Madej B, Merz KM, Monard G, Needham P, Nguyen HT, Omelyan I, Onufriev A, Roe DR, Roitberg A, Salomon-Ferrer R, Simmerling CL, Smith W, Swails J, Walker RC, Wang J, Wolf RM, Wu X, York DM, Kollman PA. 2015. AMBER 2015. University of California, San Francisco. *Available at* http://ambermd.org/doc12/Amber15.pdf (accessed 18 July 2016)

Chung SY, Subbiah S. 1996. A structural explanation for the twilight zone of protein sequence homology. *Structure.* 4:1123–1127. DOI:10.1016/S0969-2126(96)00119-0.

PeerJ Preprints | https://doi.org/10.7287/peerj.preprints.2397v2 | CC BY 4.0 Open Access | rec: 25 Jan 2017, publ: 25 Jan 2017

Devine EL, Theobald DL, Oprian DD. 2016. Relocating the Active-Site Lysine in Rhodopsin: 2. Evolutionary Intermediates. *Biochemistry*. DOI:10.1021/acs.biochem.6b00478.

Edgar RC, Drive RM, Valley M. 2004. MUSCLE: multiple sequence alignment with high accuracy and high throughput. *Nucleic Acids Research.* 32:1792–1797. DOI:10.1093/nar/gkh340.

Eddy SR. 2011. Accelerated Profile HMM Searches. *PLoS Computational Biology.* 7:e1002195. DOI:10.1371/journal.pcbi.1002195.

Eswar N, Webb B, Marti-Renom MA, Madhusudhan MS, Eramian D, Shen M-Y, Pieper U, Sali A. 2007. Comparative protein structure modeling using MODELLER. In: Coligan JE, Dunn BM, Speicher DW &Wingfield PT, ed. *Current Protocols in Protein Science*. John Wiley & Sons, Inc, Unit 2.9. DOI:10.1002/0471140864.ps0209s50.

Federici BA. 1983. Species-specific gating of gametangial dehiscence as a temporal reproductive isolating mechanism in *Coelomomyces*. *Proceedings of the National Academy of Sciences USA.* 80:604–607.

Finn RD, Bateman A, Clements J, Coggill P, Eberhardt RY, Eddy SR, Heger A, Hetherington K, Holm L, Mistry J, Sonnhammer EL, Tate J, Punta M. 2014. Pfam: the protein families database. *Nucleic Acids Research.* 42:D222–30. DOI:10.1093/nar/gkt1223.

Hanwell MD, Curtis DE, Lonie DC, Vandermeersch T, Zurek E, Hutchison GR. 2012. Avogadro: an advanced semantic chemical editor, visualization, and analysis platform. *Journal of Cheminformatics.* 4:17. DOI:10.1186/1758-2946-4-17.

Hornak V, Abel R, Okur A, Strockbine B, Roitberg A, Simmerling C. 2006. Comparison of multiple Amber force fields and development of improved protein backbone parameters. *Proteins.* 65:712–725. DOI:10.1002/prot.21123.

Humphrey W, Dalke A, Schulten K. 1996. VMD: visual molecular dynamics. *Journal of Molecular Graphics.* 14:33–38. DOI:10.1016/0263-7855(96)00018-5.

Idnurm A, Verma S, Corrochano LM. 2010. A glimpse into the basis of vision in the kingdom Mycota. *Fungal Genetics and Biology*. 47:881–892. DOI:10.1016/j.fgb.2010.04.009.

James TY, Kauff F, Schoch CL, Matheny PB, Hofstetter V, Cox CJ, Celio G, Gueidan C, Fraker E, Miądlikowska J, Lumbsch HT, Rauhut A, Reeb V, Arnold AE, Amtoft A, Stajich JE, Hosaka K, Sung, G-H, Johnson D, O'Rourke B, Crockett M, Binder M, Curtis JM, Slot, JC, Wang Z, Wilson, AW, Schüssler A, Longcore JE, O'Donnell K, Mozley-Standridge SE, Porter D, Letcher PM, Powell MJ, Taylor JW, White MM, Griffith GW, Davies DR, Humber RA, Morton JB, Sugiyama J, Rossman AY, Rogers JD, Pfister DH, Hewitt D, Hansen K, Hambleton S, Shoemaker RA, Kohlmeyer J, Volkmann-Kohlmeyer B, Spotts RA, Serdani M, Crous PW, Hughes KW, Matsuura K, Langer E, Langer G, Untereiner WA, Lücking R, Büdel B, Geiser DM, Aptroot A, Diederich P, Schmitt I, Schultz M, Yahr R, Hibbett DS, Lutzoni F, McLaughlin

PeerJ Preprints | https://doi.org/10.7287/peerj.preprints.2397v2 | CC BY 4.0 Open Access | rec: 25 Jan 2017, publ: 25 Jan 2017

DJ, Spatafora JW, Vilgalys R. 2006. Reconstructing the early evolution of Fungi using a six-gene phylogeny. *Nature.* 443:818-822. DOI:10.1038/nature05110.

James TY, Pelin A, Bonen L, Ahrendt S, Sain D, Corradi N, Stajich JE. 2013. Shared signatures of parasitism and phylogenomics unite Cryptomycota and Microsporidia. *Current Biology*. 23:1548-1553. DOI:10.1016/j.cub.2013.06.057.

Jones MDM, Forn I, Gadelha C, Egan MJ, Bass D, Massana R, Richards, TA. 2011. Discovery of novel intermediate forms redefines the fungal tree of life. *Nature*. 474:200-203. DOI:10.1038/nature09984.

Katoh K, Kuma K-I, Toh H, Miyata T. 2005. MAFFT version 5: improvement in accuracy of multiple sequence alignment. *Nucleic Acids Research.* 33:511–518. DOI:10.1093/nar/gki198.

Katoh K, Misawa K, Kuma K-I, Miyata T. 2002. MAFFT: a novel method for rapid multiple sequence alignment based on fast Fourier transform. *Nucleic Acids Research.* 30: 3059–3066. DOI:10.1093/nar/gkf436.

Katritch V, Cherezov V, Stevens RC. 2013. Structure-Function of the G Protein–Coupled Receptor Superfamily. *Annual Review of Pharmacology and Toxicology.* 53:531–556. DOI:10.1146/annurev-pharmtox-032112-135923.

Krishnan A, Almén MS, Fredriksson R, Schiöth HB. The origin of GPCRs: identification of mammalian like Rhodopsin, Adhesion, Glutamate and Frizzled GPCRs in fungi. *PLoS One.* 7:e29817. DOI:10.1371/journal.pone.0029817.

Lagerström MC, Schiöth HB. 2008. Structural diversity of G protein-coupled receptors and significance for drug discovery. *Nature Reviews Drug Discovery.* 7:339–357. DOI:10.1038/nrd2518.

Laskowski RA, MacArthur MW, Moss DS, Thornton JM. 1993. PROCHECK: a program to check the stereochemical quality of protein structures. *Journal of Applied Crystallography*. 26: 283–291. DOI:10.1107/S002188989200994.

Le Guilloux V, Schmidtke P, Tuffery P. 2009. Fpocket: an open source platform for ligand pocket detection. *BMC Bioinformatics.* 10:168. DOI:10.1186/1471-2105-10-168.

Lu M, Dousis AD, Ma J. 2008. OPUS-Rota: a fast and accurate method for side-chain modeling. *Protein Science.* 17:1576–1585. DOI:10.1110/ps.035022.108.

Lüthy R, Bowie JU, Eisenberg D. 1992. Assessment of protein models with three-dimensional profiles. *Nature*. 356:83–85. DOI:10.1038/356083a0.

Morris GM, Huey R, Lindstrom W, Sanner MF, Belew RK, Goodsell DS, Olson AJ. 2009. AutoDock4 and AutoDockTools4: Automated Docking with Selective Receptor Flexibility. *Journal of Computational Chemistry.* 30:2785–2791. DOI:10.1002/jcc.21256.AutoDock4.

PeerJ Preprints | https://doi.org/10.7287/peerj.preprints.2397v2 | CC BY 4.0 Open Access | rec: 25 Jan 2017, publ: 25 Jan 2017

Muehlstein LK, Amon JP, Leffler DL. 1987. Phototaxis in the Marine Fungus *Rhizophydium littoreum*. *Applied Environmental Microbiology.* 53:1668–1672.

Murakami M, Kouyama T. 2008. Crystal structure of squid rhodopsin. *Nature*. 453:363-367. DOI:10.1038/nature06925.

Neves SR, Ram PT, Iyengar R. 2002. G protein pathways. *Science.* 296:1636–1639. DOI:10.1126/science.1071550.

Notredame C, Higgins DG, Heringa J. 2000. T-Coffee: A novel method for fast and accurate multiple sequence alignment. *Journal of Molecular Biology.* 302:205–217. DOI:10.1006/jmbi.2000.4042.

Onufriev A, Bashford D, David A. 2000. Modification of the generalized Born model suitable for macromolecules. *Journal of Physical Chemistry B.* 104:3712–3720. DOI:10.1021/jp994072s.

Ray A, Lindahl E, Wallner B. 2010. Model quality assessment for membrane proteins. *Bioinformatics*. 26:3067-3074. DOI:10.1093/bioinformatics/btq581.

Ramachandran GN, Ramakrishnan C, Sasisekharan V. 1963. Stereochemistry of polypeptide chain configurations. *Journal of Molecular Biology.* 7:95–99.

Royant A, Nollert P, Edman K, Neutze R, Landau EM, Pebay-Peyroula E, Navarro J. 2001. X-ray structure of sensory rhodopsin II at 2.1-Å resolution. *Proceedings of the National Academy of Sciences USA.* 98:10131-10136. DOI:10.1073/pnas.181203898.

Sali A. 1995. Modeling mutations and homologous proteins. *Current Opinion in Biotechnology*. 6:437-451. DOI:10.1016/0958-1669(95)80074-3.

Saranak J, Foster KW. 1997. Rhodopsin guides fungal phototaxis. *Nature.* 387:465–466. DOI:10.1038/387465a0.

Schweiger U, Tittor J, Oesterhelt D. 1994. Bacteriorhodopsin can function without a covalent linkage between retinal and protein. *Biochemistry*. 33:535-541.

Sekharan S, Morokuma K. 2011. Why 11-*cis*-Retinal? Why Not 7-*cis*, 9-*cis*, or 13-*cis*-Retinal in the Eye? *Journal of the American Chemical Society.* 133:19052-19055. DOI:10.1021/ja208789h.

Shen M-Y, Sali A. 2006. Statistical potential for assessment and prediction of protein structures. *Protein Science.* 15:2507–2524. DOI:10.1110/ps.062416606.

Shichida Y, Matsuyama T. 2009. Evolution of opsins and phototransduction. *Philosophical Transactions of the Royal Society B: Biological Sciences*. 364: 2881–2895. DOI:10.1098/rstb.2009.0051.

PeerJ Preprints | https://doi.org/10.7287/peerj.preprints.2397v2 | CC BY 4.0 Open Access | rec: 25 Jan 2017, publ: 25 Jan 2017

596 Slater GS, Birney E. 2005. Automated generation of heuristics for biological sequence
597 comparison. *BMC Bioinformatics.* 6:31-41. DOI:10.1186/1471-2105-6-31.
598
599 Smith SO. 2010. Structure and activation of the visual pigment rhodopsin. *Annual Review of*
600 *Biophysics*. 2010;39: 309–328. DOI:10.1146/annurev-biophys-101209-104901.
601
602 Spudich JL, Yang CS, Jung KH, Spudich EN. 2000. Retinylidene proteins: structures and
603 functions from archaea to humans. *Annual Review of Cell and Developmental Biology.* 16:365–
604 392. DOI:10.1146/annurev.cellbio.16.1.365.
605
606 Stajich JE, Berbee ML, Blackwell M, Hibbett DS, James TY, Spatafora JW, Taylor JW. 2009.
607 The Fungi. *Current Biology.* 19:R840-5. DOI:10.1016/j.cub.2009.07.004.
608
609 Taddese B, Simpson LM, Wall ID, Blaney FE, Reynolds CA. 2013. Modeling Active GPCR
610 Conformations. In: Conn PM, ed. *Methods in Enzymology.* Academic Press. 2:21-35.
611 DOI:10.1016/B978-0-12-407865-9.00002-9.
612
613 Terakita A. 2005. The opsins. *Genome Biology*. 6:213. DOI:10.1186/gb-2005-6-3-213.
614
615 Wang J, Wolf RM, Caldwell JW, Kollman PA, Case DA. 2004. Development and testing of a
616 general amber force field. *Journal of Computational Chemistry*. 25:1157–1174.
617 DOI:10.1002/jcc.20035.
618
619 Wiederstein M, Sippl MJ. 2007. ProSA-web: interactive web service for the recognition of errors
620 in three-dimensional structures of proteins. *Nucleic Acids Research*. 35:W407–10.
621 DOI:10.1093/nar/gkm290.
622
623
624 Zhang F, Vierock J, Yizhar O, Fenno LE, Tsunoda S, Kianianmomeni A, Prigge M, Berndt A,
625 Cushman J, Polle J, Magnuson J, Hegemann P, Deisseroth K. The microbial opsin family of
626 optogenetic tools. *Cell.* 147:1446-1457. DOI:10.1016/j.cell.2011.12.004
627
628 Zhang J, Zhang Y. 2010. GPCRRD: G protein-coupled receptor spatial restraint database for 3D
629 structure modeling and function annotation. *Bioinformatics.* 23:3004-5. DOI:
630 10.1093/bioinformatics/btq563

PeerJ Preprints | https://doi.org/10.7287/peerj.preprints.2397v2 | CC BY 4.0 Open Access | rec: 25 Jan 2017, publ: 25 Jan 2017

S. punctatus	13-*cis*-retinal	9-*cis*-retinal	3,4-dehydro-retinal	3-hydroxy-retinal	4-hydroxy-retinal	all-*trans*-retinal	11-*cis*-retinal
State 0	24.52	6.77	24.06	24.23	24.81	23.44	10.07
State 1	0.31	-1.56	-2.02	-1.37	-1.30	-1.78	-0.68
State 2	-1.96	-2.72	-2.15	-2.31	-2.58	-2.41	-1.78
State 3	-2.11	-0.35	0.43	0.20	0.47	0.42	-2.11
State 4	-1.76	-1.83	-0.82	-0.48	-1.15	-1.03	-1.49
T. pacificus	13-*cis*-retinal	9-*cis*-retinal	3,4-dehydro-retinal	3-hydroxy-retinal	4-hydroxy-retinal	all-*trans*-retinal	11-*cis*-retinal
State 0	-2.83	-5.43	-4.52	-2.94	-3.20	-4.83	-5.66
State 1	-0.91	-3.84	-3.66	-3.40	-3.30	-3.78	-1.88
State 2	-4.57	-2.25	-4.74	-4.24	-4.40	-4.73	-4.17
State 3	-3.79	-2.43	-2.82	-1.95	-2.56	-2.87	-3.52
State 4	0.27	-0.80	-1.04	-0.69	-0.75	-1.02	-0.21

Table 1. Autodock results (binding energies in kcal/mol) for the *S. punctatus* homology model and *T. pacificus* crystal structure (PDB ID: 2Z73) with retinal isomers before and after molecular mechanics simulations. Values represent free energy of the lowest scoring conformation (in kcal/mol). "State 0" refers to the model state prior to the start of MD simulations. States "1", "2", "3", and "4" refer to snapshot states immediately after start of MD, and at every 25ns thereafter. During the course of the simulation, the free energy of binding is minimized for both the 13-*cis*- and 9-*cis*-retinal isomers with the *S. punctatus* homology model. For *T. pacificus*, State 0 represents the experimentally verified crystal structure, published in complex with 11-*cis*-retinal (Murakami & Kouyama 2008).

Outline / notes

Draft text

Fig 1. Structural details of the *S. punctatus* homology model. A) Structural alignment of *S. punctatus* homology model (grey) with *T. pacificus* crystal structure (light purple). S*. punctatus* residues are colored according to function: orange (binding pocket residues), red (putative counterion), purple (disulfide bond), yellow (salt bridge), dark blue (NPxxY motif), and pink & black (ion lock). Inset figures provide details for structural alignments of *S. punctatus* and *T. pacificus* B) disulfide bond and salt bridge regions, C) binding pocket residues, and D) ERY and NPxxY regions.

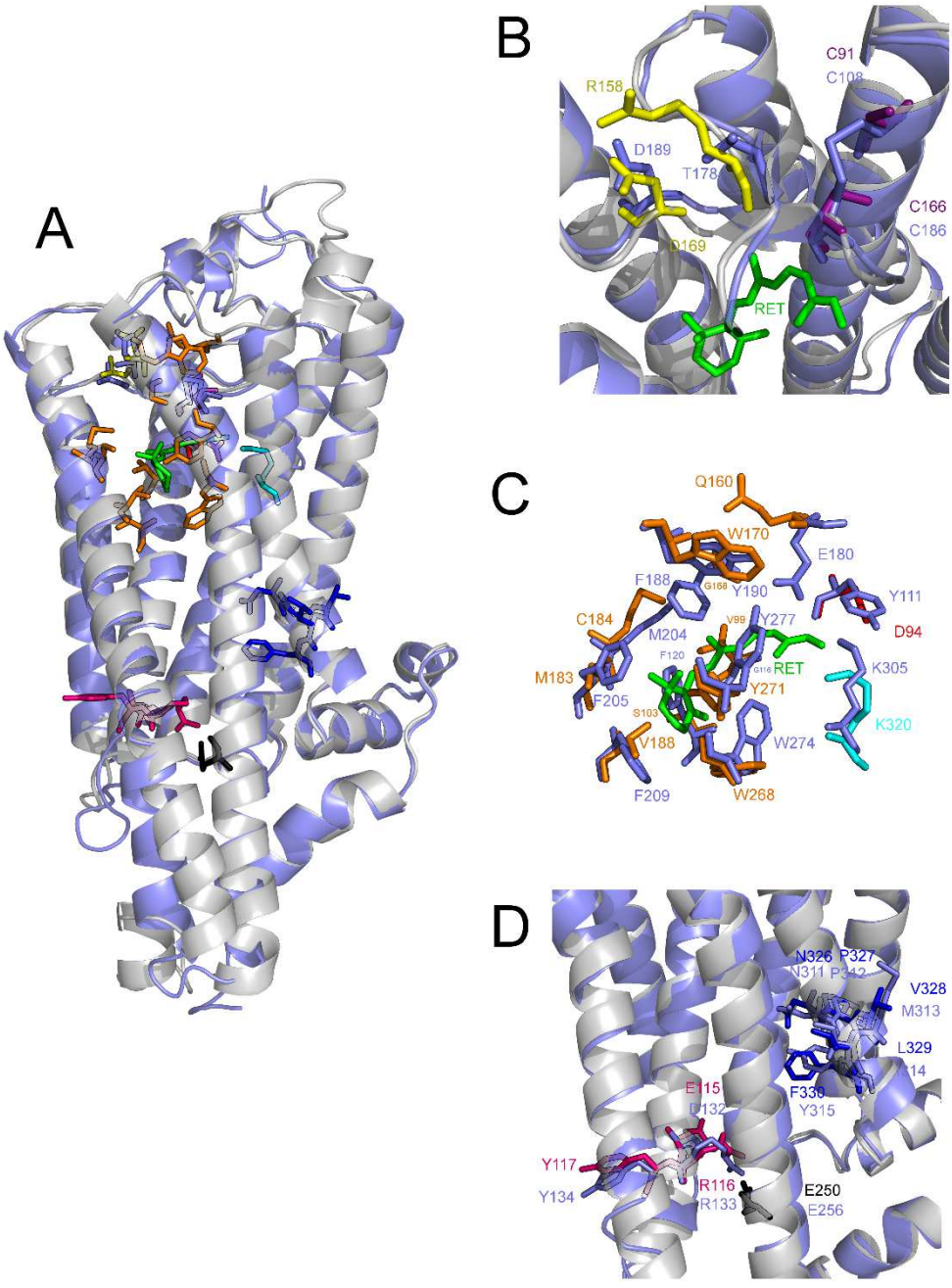

Outline / notes

Draft text

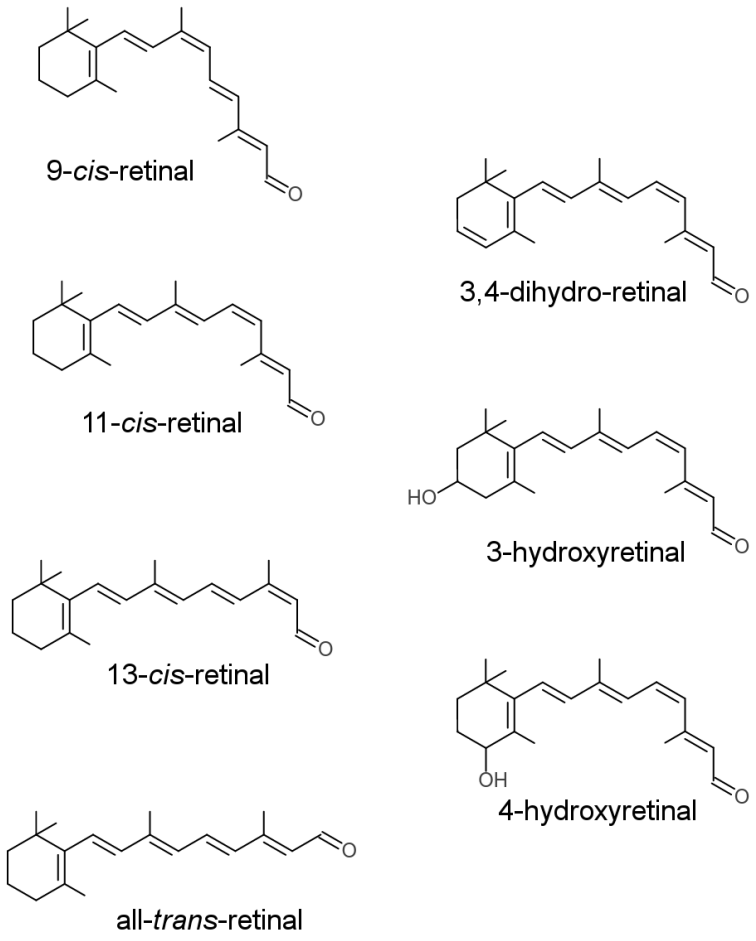

Fig2. Retinaldehyde chromophores used by opsins. Each isomer was used in an in silico docking screen against the *S. punctatus* homology model and the *T. pacificus* rhodopsin crystal structure (PDBID 2Z73)

Outline / notes

Draft text

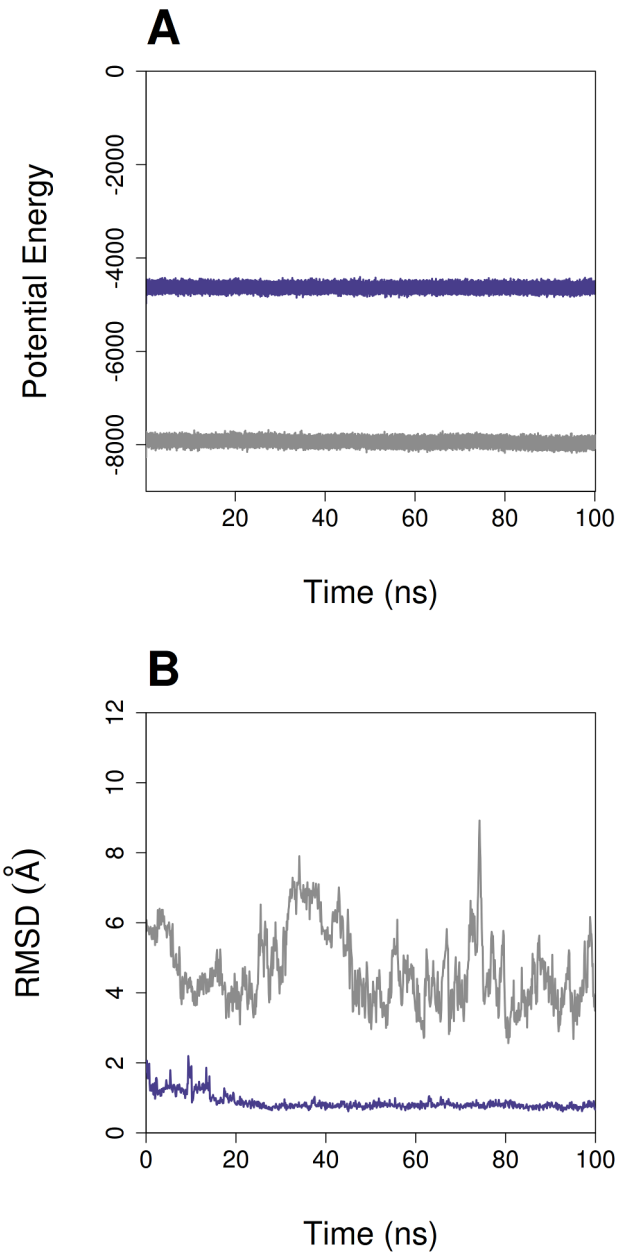

Fig 3. Overview plots of MD simulation runs of *T. pacificus* (squid) crystal structure with 11-*cis*-retinal (purple) and *S. punctatus* (fungal) model with 9-*cis*-retinal (gray). A) Over the course of the simulation, the potential energy of both structures remains relatively stable. The fungal structure has substantially lower potential energy than the squid structure. B) While the average RMSD of the fungal structure is higher and more variable than that of the squid, both are relatively stable during the simulation.

Outline / notes

Draft text

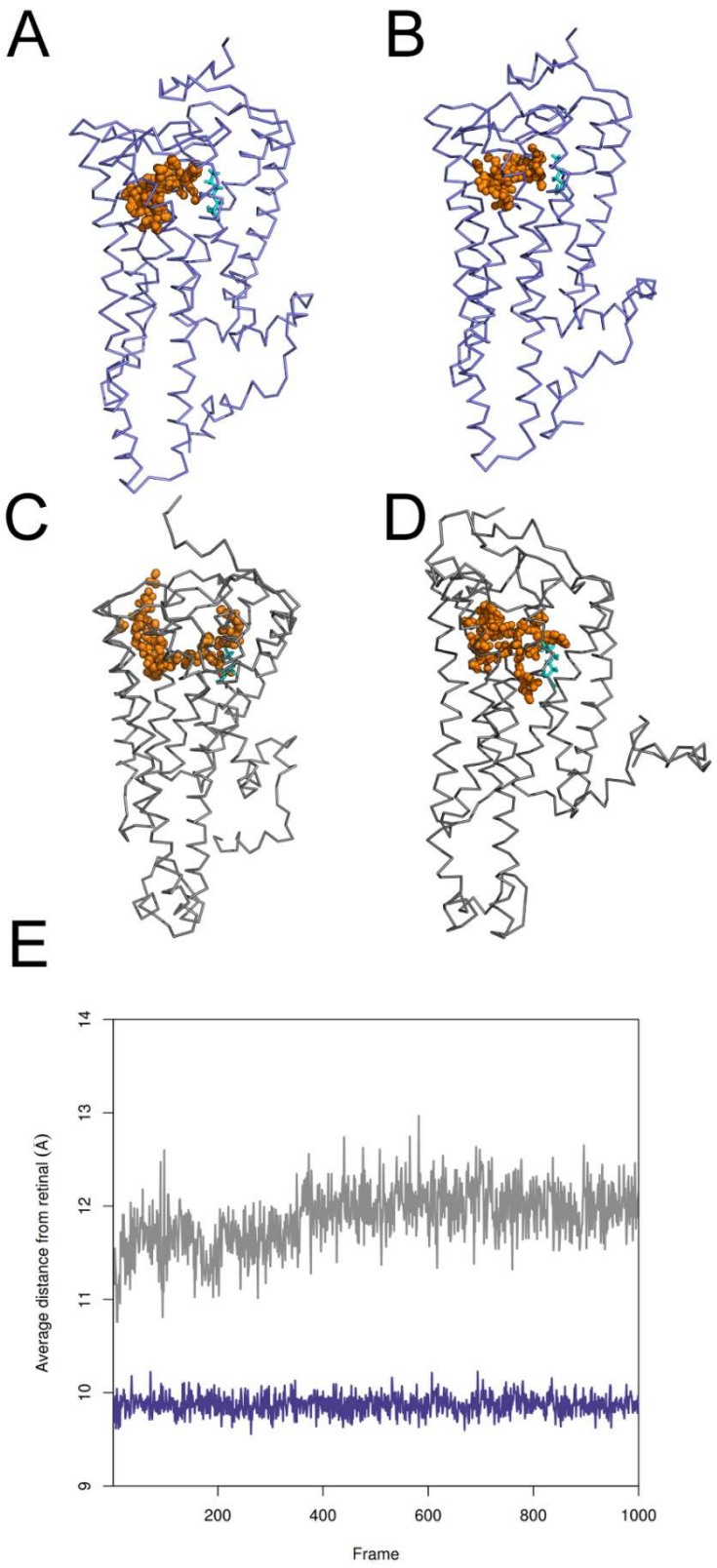

Fig 4. Changes in receptor binding pockets of *T. pacificus* and *S. punctatus* structures during MD simulations. A-D) Pockets generated by Fpocket server are represented as colored clusters of spheres. The conserved lysine residue is represented in cyan. Initial configurations of *T. pacificus* (purple) and *S. punctatus* (gray) are displayed in A) and C), respectively. Likewise, final conformations after 100ns MD simulations are displayed in B) and D) for *T. pacificus* and *S. punctatus*, respectively. E) Average distance between the retinal ligand center-of-mass and each of the binding pocket residues, as measured in both *T. pacificus* crystal structure (purple) and *S. punctatus* homology model (gray) over the course of the 100ns molecular dynamics simulation.

Outline / notes

Draft text

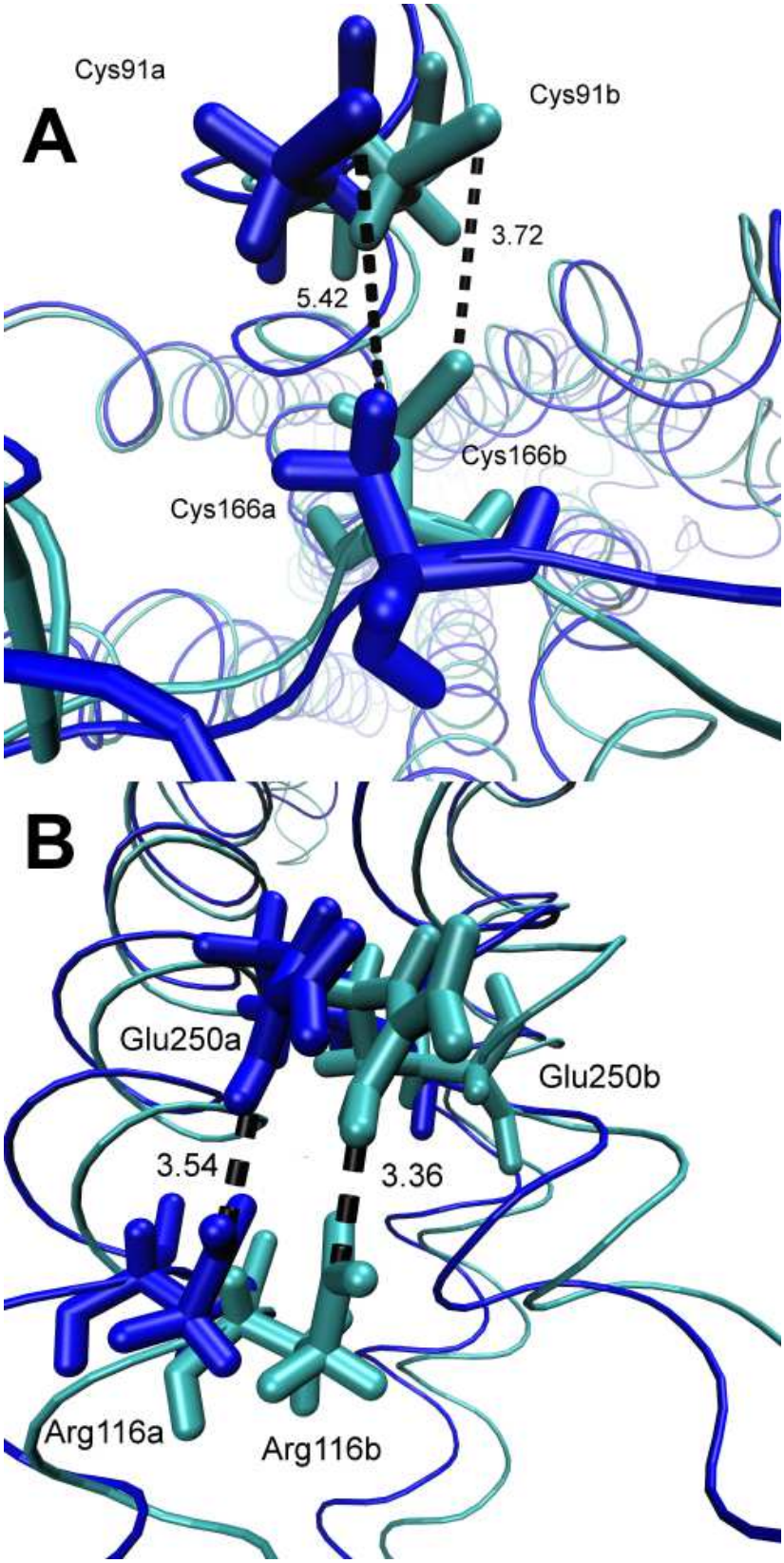

Fig 5. Change in distances between the A) cysteine-cysteine disulfide bond and B) ion lock structural motifs during the *S. punctatus* 100ns MD simulation. Initial conformations are represented in dark blue with residue designations of “a”. Final conformations are represented in cyan with residue designations of “b”.

Outline / notes

Draft text

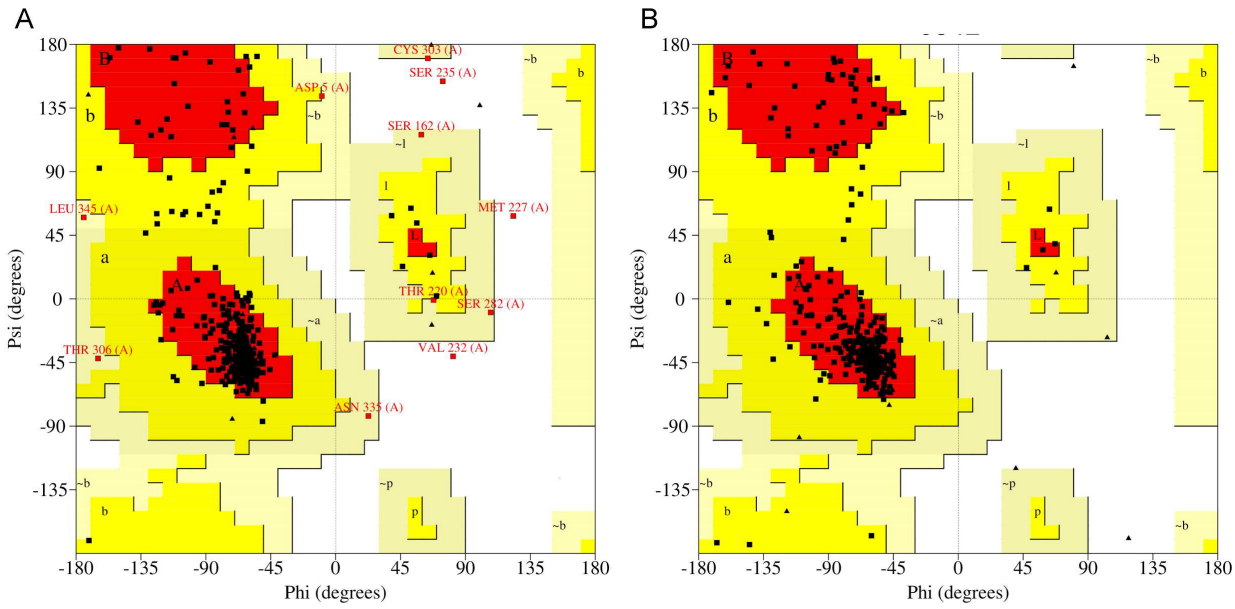

Fig S1. PROCHECK-generated Ramachandran plots for a) *S. punctatus* iTasser homology model and B) *T. pacificus* rhodopsin x-ray crystal structure (PDB ID: 2Z73).

Outline / notes

Draft text

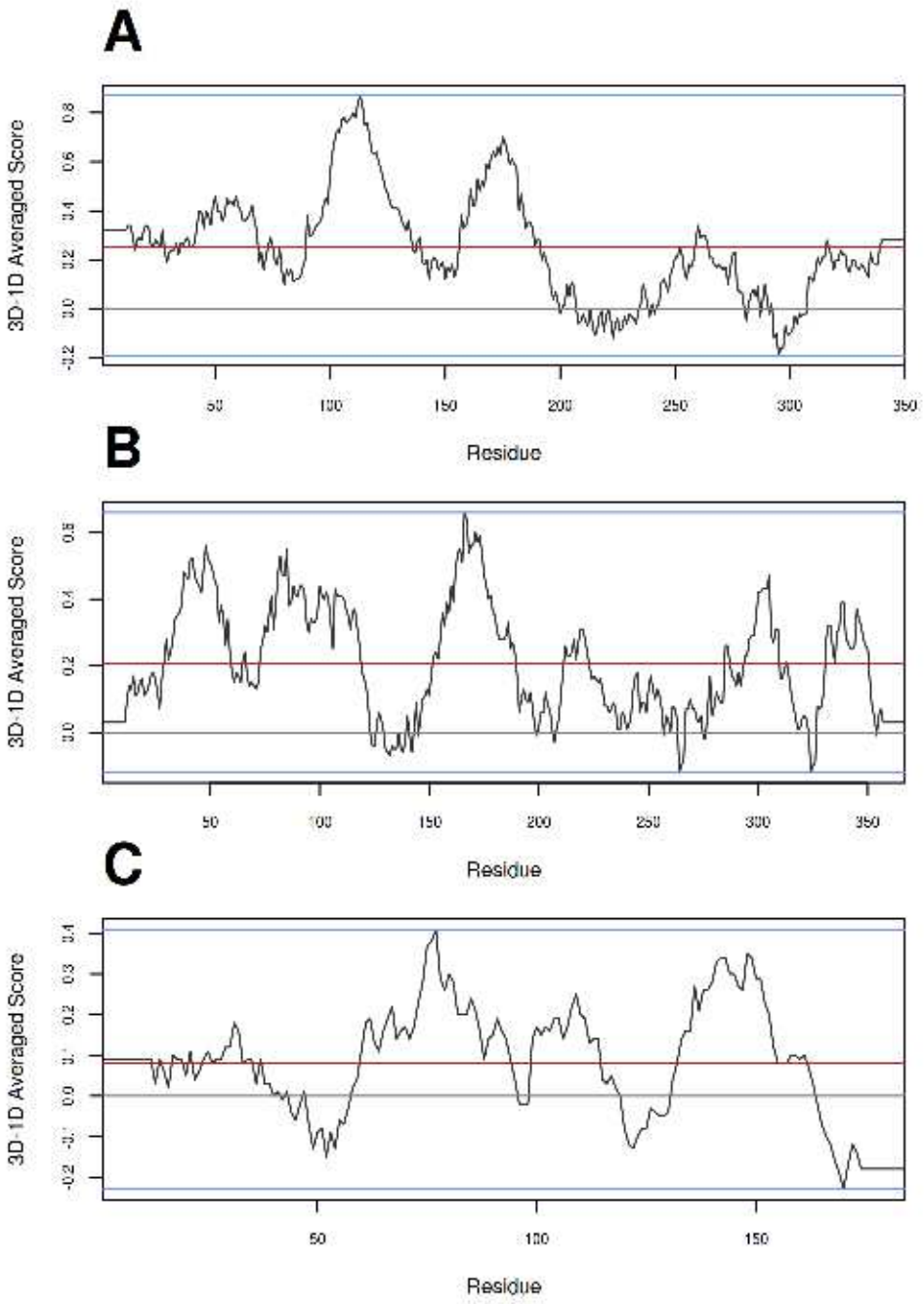

Figure S2. 3D-1D averaged scores across the length of A) the *T. pacificus* crystal structure, B) the *S. punctatus* homology model against the iTasser GPCR database, and C) the *S. punctatus* homology model against the sensory rhodopsin II xray crystal structure from the archaeon *Natronomonas pharaonis* (PDBid 1H68). Far more residues have averaged scores below 0 in the *S. punctatus* model using 1H68 as the template than in the other two structures.

Outline / notes

Draft text

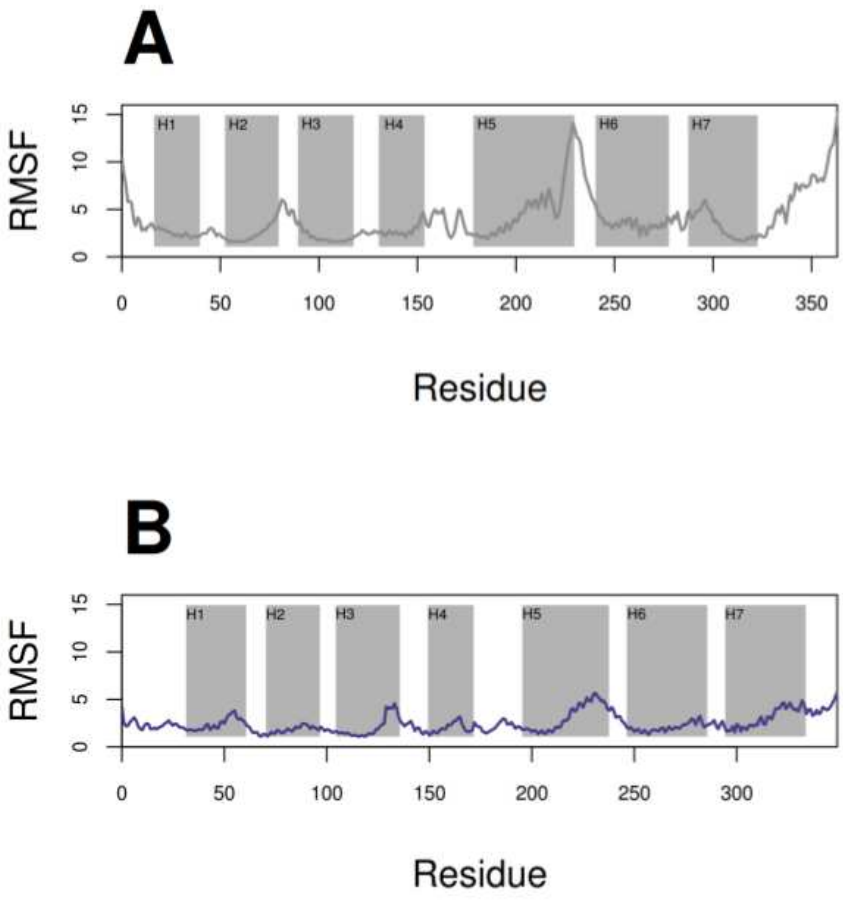

Figure S3.
Average root mean square deviation for each residue position during the 100ns simulation. Helical regions are annotated with rectangles. A) *S. punctatus* model B) *T. pacificus* crystal structure.

Outline / notes

Draft text

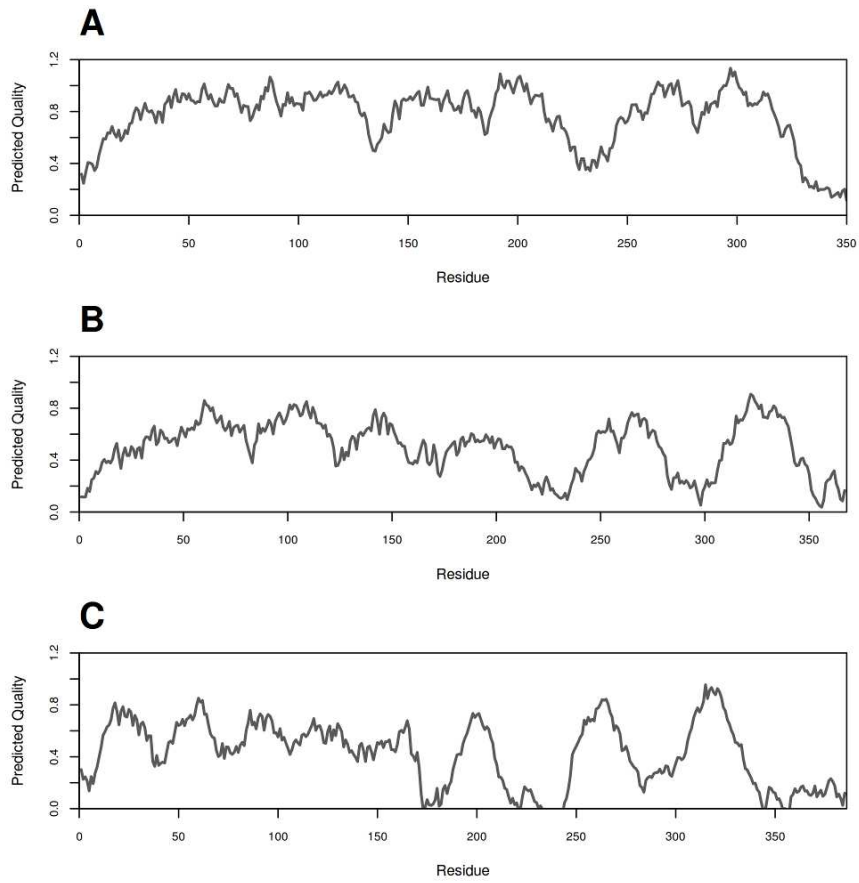

Figure S4. Quality assessment using ProQM for A) the *T. pacificus* crystal structure, B) the *S. punctatus* homology model against the iTasser GPCR database, and C) the *S. punctatus* homology model against the sensory rhodopsin II xray crystal structure from the archaeon *Natronomonas pharaonis* (PDBid 1H68). The global quality score for the fungal sequence against the sensory rhodopsin template was lower than that of the iTasser fungal model.